Volume 15, Issue 3, 152534 (1-14)

Iranian Journal of Catalysis (IJC)

https://doi.org/10.57647/j.ijc.2025.1503.34

$CuNiP_2O_7/CuFe_2O_4$ as magnetically separable solid acid nanocatalyst for synthesis of 1-Amidoalkyl-2-naphthols

Elnaz Ghafouri[1], Abdolhamid Bamoniri[1,*], Bi Bi Fatemeh Mirjalili[2]

[1]*Department of Organic Chemistry, Faculty of Chemistry, University of Kashan, Kashan, Iran.*
[2]*Department of Chemistry, College of Science, Yazd University, Yazd, Iran.*

[*]**Corresponding author:** bamoniri@kashanu.ac.ir

Original Research

Received:
12 February 2025
Revised:
5 June 2025
Accepted:
30 June 2025
Published online:
1 July 2025
Published in issue:
31 September 2025

Abstract:

There is increasing interest in the environmentally friendly synthesis of nanoparticles. In this regard, we report a green method to prepare a novel metal diphosphate nanocatalyst, $CuNiP_2O_7$, using ginger extract as a stabilizing agent. The nanocatalyst was further decorated with $CuFe_2O_4$ to obtain a magnetically separable nanocatalyst. Characterization was performed using XRD, FESEM, EDX, FTIR, and Raman analyses. The FESEM image clearly reveals the effectiveness of the ginger extract in synthesizing uniformly sized nanoparticles. FT-IR and Raman spectroscopy confirmed the formation of metal-phosphate bonds acting as strong acid sites. The nanocatalyst efficiently facilitated the three-component synthesis of 1-amidoalkyl-2-naphthol under solvent-free conditions, with the best results obtained at an optimized temperature of 90 °C and a reaction time of only 10 min. The optimum amount of the nanocatalyst was found to be 0.04 g, leading to a high yield of 97%. The reusability of the nanocatalyst was confirmed through five successive reaction cycles without significant loss of activity. Various derivatives of amidoalkyl-2-naphthol were successfully synthesized using the prepared nanocatalyst.

Keywords: $CuNiP_2O_7$; Nanocatalyst; Ginger extract; Three-component reaction; 1-amidoalkyl-2-naphthol; Solvent-less

1. Introduction

Owing to their superior pharmaceutical applications, 1-amidoalkyl-2-naphthols have been synthesized for many decades. They have offered a variety of properties, including nucleoside antibiotics and HIV protease inhibitors [1–4]. Because of their importance, high-yield synthesis of 1-amidoalkyl-2-naphthols is of great interest. The common synthesis method for 1-amidoalkyl-2-naphthols is a three-component condensation reaction between 2-naphthol, amide, and aldehyde. Three-component reaction is categorized as a multi-component reaction where three or more reactants react in a single step to form a product. These reactions occupy a great position in drug and natural product synthesis, such as Ugi reaction, Biginelli reaction, and Passerini, due to their high efficiency and feasibility for the synthesis of various compounds [5, 6].

Different homogenous and heterogeneous catalysts, such as sulfonic acid [7], phosphoric acid [8], SiO_2-$NaHSO_4$ [9], $Mg(ClO_4)_2$ [10], ZnO/CuO [11], and Ag/TiO_2 [12] nanoparticles have been used to prompt the synthesis reaction of 1-amidoalkyl-2-naphthols. However, the homogeneous catalysis of the condensation reaction requires time-consuming separation of the catalyst and purification of the product, which limits its uses to facilitate the reaction. Hence, heterogeneous catalysis has gained great attention because of the ease of recovery and reusability of the catalyst, as well as the need for less amount of reagents.

In this regard, metal diphosphate compounds with the general formula of $A_2P_2O_7$ (A = divalent ions = Ca, Mg, Cu, Ni, etc.) can serve as efficient catalysts [13, 14]. Metal diphosphates form a layered structure composed of alternating AO_5 and PO_4 polyhedral layers. These compounds can exhibit acidity (Lewis or Brønsted), basicity, or redox properties, which are crucial for being potential catalyst materials [15, 16]. Spielbauer et al. suggested that the P(OH) groups act as Brønsted acid, while metal ions are considered as Lewis acid [17, 18]. Owing to their excellent

physicochemical properties, these compounds are involved in various applications, especially in catalytic reactions [19–21]. As a heterogeneous catalyst, metal diphosphates play the key role in organic chemistry and the preparation of fine chemicals [22]. For instance, Guo et al. reported the dehydration of lactic acid to acrylic acid using lanthanum phosphate catalyst [23]. Weingarten et al. prepared zirconium phosphate catalyst and studied its catalytic potential for the conversion of glucose into levulinic acid [24]. In addition, Drici et al. utilized iron phosphate nanoparticles for the catalytic synthesis of propargylamine [25]. Also, enantioselective Muaiyama-Michael reaction between β, γ-unsaturated α-ketoesters and silyl ketene acetals has been studied using chiral magnesium phosphate [26].

Green chemistry by employing natural compounds has extended our insight for the synthesis of nanomaterials without posing a big threat to the environment [27]. In this case, the capability of using plant and flower extracts as reducing or capping agents has been recognized, due to the presence of substantial amounts of phenolic compounds, alkaloids, terpenoids, and proteins [28, 29]. Particularly, ginger extract contains a variety of ingredients, including gingerols, shogaols, gingediols, and gingediacetates, serving as the stabilizing agents for the preparation of the nanoparticles [30–32].

Herein, we have been reported the preparation of $CuNiP_2O_7$ (CNPO) nanoparticles using ginger extract. In order to ease the catalyst separation from the reaction media, the CNPO was decorated with prepared $CuFe_2O_4$ (CFO) magnetic nanoparticles. Amidoalkyl-2-naphthol derivatives were synthesized through the three-component reaction using the prepared CNPO/CFO nanocatalyst. For comparison, the CNPO catalyst was also prepared in aqueous media, and studied its effect on the yield of the synthesis of amidoalkyl-2-naphthol was studied. Different experimental conditions, including the amount of loaded nanocatalyst, type of solvent, temperature, and reaction time, were studied to achieve a higher yield of products. Scheme 1 represents the overall overview for the synthesis of 1-amidoalkyl-2-naphtol using the prepared CNPO/CFO nanocatalyst.

2. Experimental

2.1 Preparation of nanocatalyst

2.1.1 Preparation of $CuNiP_2O_7$

A green approach was used to the synthesis of $CuNiP_2O_7$ (CNPO). At first, the aqueous extract of ginger was prepared. For that, 5.0 g of ginger powder was distributed into 100 mL of deionized water. The mixture was then heated at 60 °C for 2 hours. The light yellow solution was filtered using Whatman filter paper and stored in a refrigerator for subsequent use in the preparation of CNPO as the green stabilizing agent.

1 mmol of $Cu(NO_3)_2{\cdot}3H_2O$, 1 mmol of $Ni(NO_3)_2{\cdot}6H_2O$, and 2 mmol of $H_2NH_4PO_4$ were dissolved in 50 mL of the as-prepared ginger extract. The solution was extremely stirred and heated above 50 °C until complete evaporation of the water. Then, the light yellow solid was collected and calcined at 800 °C for 7 hours. A similar procedure was followed to prepare CNPO in pure distilled water media instead of using ginger extract solution. Scheme 2 typically exhibits how gingerol compounds within the ginger extract surround CNPO nanoparticles, impeding their accumulation and growth to form micro-sized particles.

2.1.2 Preparation of the $CuFe_2O_4$

The facile and straight co-precipitation method was employed to prepare the $CuFe_2O_4$ nanoparticles (CFO). At first, 1 mmol of $Cu(NO_3){\cdot}3H_2O$ and 2 mmol of $Fe(NO_3){\cdot}9H_2O$ were dissolved in 20 mL of deionized water. The solution was added dropwise to another solution containing 4 mL of PEG (MW = 400) and 50 mL of deionized water. After that, NaOH solution (0.1 M) was added dropwise until reaching pH 8. The mixture was stirred for about 30 minutes and then dried at 90 °C overnight. The dried solid product was calcined at 500 °C for 4 hours to achieve the pure CFO nanoparticles [33].

2.1.3 Preparation of CNPO/CFO magnetic nanocatalyst

In order to prepare a magnetically separable nanocatalyst, the CFO nanoparticles were anchored on the surface of the as-prepared CNPO. For this purpose, we used the simple route for the combination of both materials in which 0.3 g of the as-prepared CNPO and 0.1 gr CFO nanoparticles were well mixed in a mortar for around 1 hour. Then, the resulted powder was calcined at 800 °C for 7 hours.

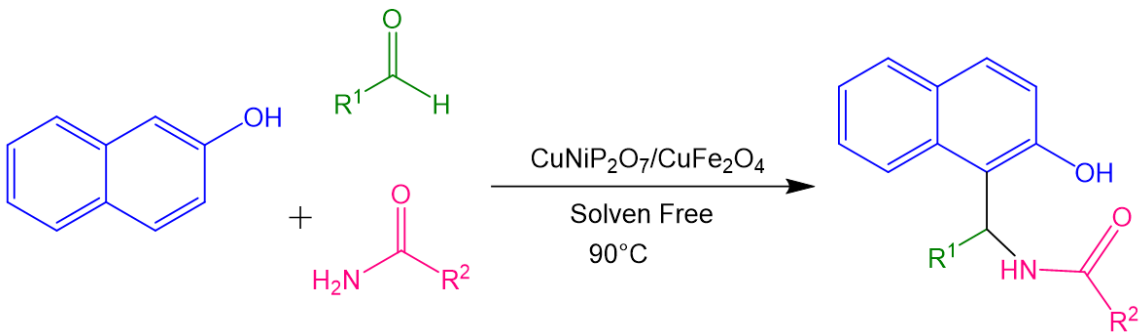

Scheme 1. Synthesis of 1-amidoalkyl-2-naphtol using the prepared CNPO/CFO nanocatalyst.

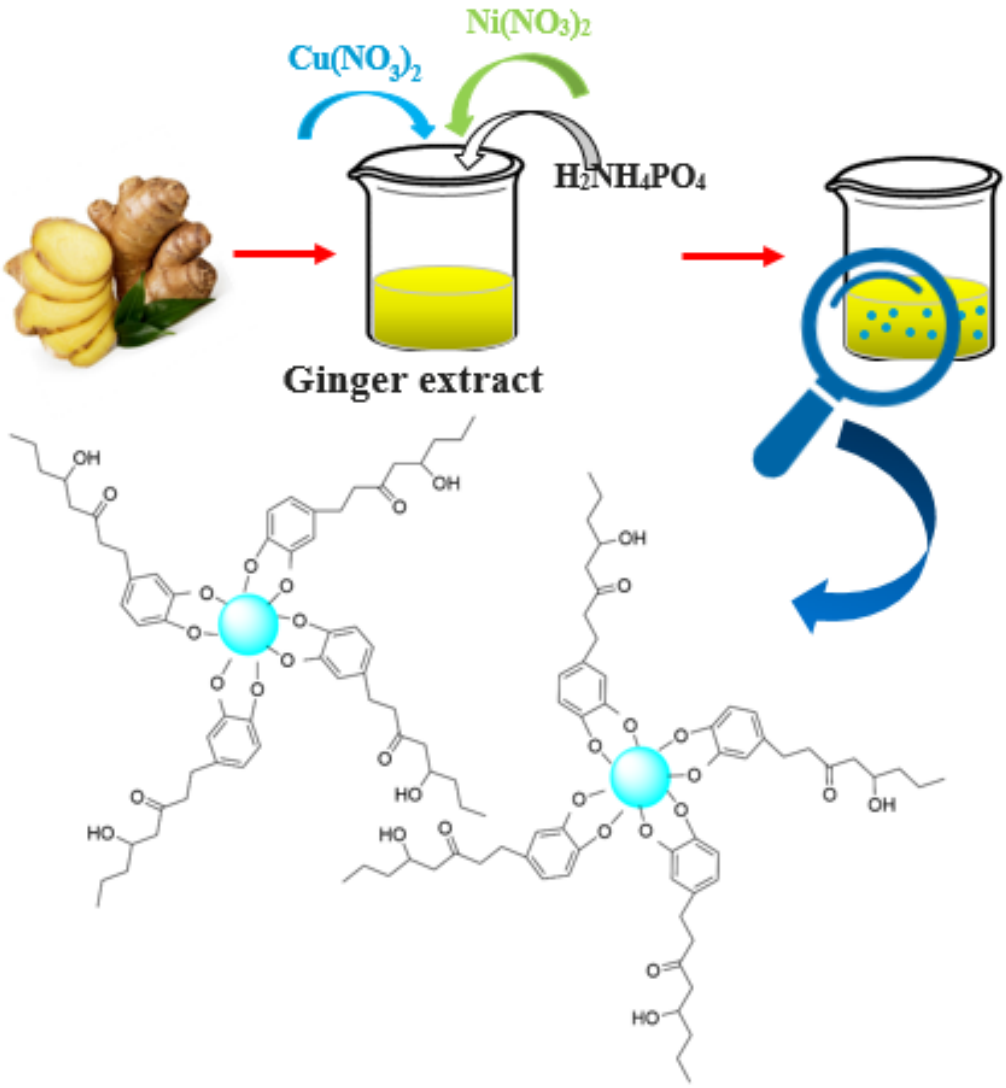

Scheme 2. A description for stabilization of $CuNiP_2O_7$ by gingerol compound within the ginger extract.

2.2 Synthesis of 1-amidoalkyl-2-naphthols using CNPO/CFO nanocatalyst

The three-component reaction was utilized in order to synthesize of 1-amidoalkyl-2-naphthols. The mixture containing 2 mmol of 2-naphthol, 1 mmol of amide and 1 mmol of an aromatic aldehyde were heated at 90 °C in the presence of CNPO/CFO magnetic nanocatalyst (0.04 g). The progress of the reaction was investigated using TLC. The reaction mixture was stirred at a constant temperature for about 30 minutes. After that, the obtained solid was dissolved in deionized water, and then the nanocatalyst were separated by a bar magnet. The product was crystallized from the methanol and then dried in a desiccator.

2.3 Spectroscopic data for the synthesized 1-amidoalkyl-2-naphthols

The synthesized 1-amidoalkyl-2-naphthol derivatives were analyzed using ^{1}H NMR, ^{13}C NMR, and FTIR, which are provided as follows:

N-[(2-Hydroxynaphthalene-1-yl)-(phenyl)-methyl]-benzamide

^{1}H NMR (400 MHz, DMSO-d_6) δ 10.34 (s, 1H), 9.03 (d, J = 8.4 Hz, 1H), 8.09 (d, J = 8.7 Hz, 1H), 7.87 (d, J = 7.7 Hz, 2H), 7.84 – 7.79 (m, 2H), 7.56 (t, J = 7.2 Hz, 1H), 7.49 (d, J = 1.6 Hz, 3H), 7.33 – 7.28 (m, 7H), 7.25 (d, J = 8.8 Hz, 1H). FTIR (KBr pellets ν (cm^{-1})) 701, 753, 822, 1435, 1531, 1627, 3067, 3041.

N-[(2-Hydroxynaphthalene-1-yl)- (3-nitrophenyl)-methyl]-benzamide

^{1}H NMR (400 MHz, DMSO-d_6) δ 10.42 (s, 1H), 9.15 (d, J = 8.0 Hz, 1H), 8.12 – 8.09 (m, 3H), 7.91 – 7.83 (m, 4H), 7.72 (d, J = 7.9 Hz, 1H), 7.57 (dd, J = 10.0, 6.9 Hz, 2H), 7.52 – 7.48 (m, 3H), 7.40 (d, J = 8.1 Hz, 1H), 7.34 (d, J = 7.4 Hz, 1H), 7.26 (d, J = 8.8 Hz, 1H). FTIR (KBr pellets ν (cm^{-1})) 653, 732, 812, 1280, 1341, 1428, 1520, 1631, 3270, 3420.

N-[(2-Hydroxynaphthalene-1-yl)-(4-chlorophenyl)-methyl]-benzamide

^{1}H NMR (400 MHz, DMSO-d_6) δ 10.34 (s, 1H), 9.02 (d, J = 8.5 Hz, 1H), 8.06 (d, J = 8.6 Hz, 1H), 7.84 (d, J = 13.9 Hz, 4H), 7.55 (d, J = 7.1 Hz, 1H), 7.49 (t, J = 7.2 Hz, 3H), 7.35 (d, J = 8.1 Hz, 3H), 7.29 – 7.23 (m, 4H). FTIR (KBr pellets ν (cm^{-1})) 726, 812, 873, 1264, 1336, 1438, 1512, 1627, 3115, 3389.

N-[(2-Hydroxynaphthalene-1-yl)-(2-nitrophenyl)-methyl]-benzamide

^{1}H NMR (400 MHz, DMSO-d_6) δ 9.90 (s, 1H), 9.10 (d, J = 7.7 Hz, 1H), 7.98 (d, J = 8.8 Hz, 1H), 7.91 – 7.87 (m, 2H), 7.84 – 7.73 (m, 4H), 7.62 (t, J = 7.7 Hz, 1H), 7.51 (dt, J = 9.9, 6.7 Hz, 3H), 7.46 – 7.40 (m, 3H), 7.29 (t, J = 7.5 Hz, 1H), 7.11 (d, J = 8.6 Hz, 1H). FTIR (KBr pellets ν (cm^{-1})) 706, 751, 821, 1280, 1344, 1435, 1526, 1635, 3139, 3421.

N-[(2-Hydroxynaphthalene-1-yl)-(3-ethoxy-4-hydroxyphenyl)-methyl]-benzamide

^{1}H NMR (400 MHz, DMSO-d_6) δ 10.30 (s, 1H), 9.02 (d, J = 8.6 Hz, 1H), 8.78 (s, 1H), 8.09 (d, J = 8.7 Hz, 1H), 7.85 – 7.82 (m, 3H), 7.78 (d, J = 8.9 Hz, 1H), 7.54 (d, J = 7.2 Hz, 1H), 7.48 (t, J = 7.5 Hz, 3H), 7.31 (t, J = 7.5 Hz, 1H), 7.24 (d, J = 8.9 Hz, 1H), 7.18 (d, J = 8.6 Hz, 1H), 6.93 (s, 1H), 6.65 (d, J = 2.8 Hz, 2H), 3.90 – 3.86 (m, 2H), 1.25 (d, J = 6.9 Hz, 3H). FTIR (KBr pellets ν (cm^{-1})) 714, 814, 846, 1278, 1348, 1436, 1518, 1621, 3158, 3394.

N-[(2-Hydroxynaphthalene-1-yl)-(2,4-di-chlorophenyl)-methyl]-benzamide

^{1}H NMR (400 MHz, DMSO-d_6) δ 10.30 (s, 1H), 9.02 (d, J = 8.6 Hz, 1H), 8.78 (s, 1H), 8.09 (d, J = 8.7 Hz, 1H), 7.85 – 7.82 (m, 3H), 7.78 (d, J = 8.9 Hz, 1H), 7.54 (d, J = 7.2 Hz, 1H), 7.48 (t, J = 7.5 Hz, 3H), 7.31 (t, J = 7.5 Hz, 1H), 7.24 (d, J = 8.9 Hz, 1H), 7.18 (d, J = 8.6 Hz, 1H), 6.93 (s, 1H), 6.65 (d, J = 2.8 Hz, 2H), 3.90 – 3.86 (m, 2H), 1.25 (d, J = 6.9 Hz, 3H). FTIR (KBr pellets ν (cm^{-1})) 707, 754, 822, 1276, 1346, 1438, 1530, 1682, 3072, 3421.

N-[(2-Hydroxynaphthalene-1-yl)-(phenyl)-methyl]-acetamide

^{1}H NMR (400 MHz, DMSO-d_6) δ 9.4 (S, 1H),8.45 (d, J = 8.3 Hz, 1H), 7.78 (dd, J = 16.6, 8.5 Hz, 3H), 7.36 (t, J = 7.6 Hz, 1H), 7.25 (ddd, J = 11.2, 8.4, 4.7 Hz, 4H), 7.18 – 7.12 (m, 4H), 1.98 (s, 3H). FTIR (KBr pellets ν (cm^{-1})) 724, 808, 824, 1274, 1332, 1436, 1516, 1687, 3242, 3397.

N-[(2-Hydroxynaphthalene-1-yl)-(4-nitrophenyl)-methyl]-acetamide

^{1}H NMR (400 MHz, DMSO-d_6) δ 8.59 (d, J = 8.0 Hz, 1H), 8.14 (d, J = 8.6 Hz, 2H), 7.82 (t, J = 9.0 Hz, 3H), 7.40 (d, J = 8.4 Hz, 3H), 7.29 (t, J = 7.5 Hz, 3H), 7.23 (d, J = 8.9 Hz, 1H), 7.17 (d, J = 7.8 Hz, 1H), 2.02(S, 3H). FTIR (KBr pellets ν (cm^{-1})) 751, 821, 851, 1280, 1347, 1438, 1518, 1634, 3065, 3389.

N-[(2-Hydroxynaphthalene-1-yl)-(4-chlorophenyl)-methyl]-acetamide

^{1}H NMR (400 MHz, DMSO-d_6) δ 8.48 (d, J = 8.2 Hz, 1H), 7.79 (dd, J = 14.7, 8.3 Hz, 3H), 7.38 (t, J = 7.6 Hz, 1H), 7.33 – 7.22 (m, 4H), 7.15 (d, J = 8.2 Hz, 2H), 7.08 (d, J = 8.2 Hz, 1H), 1.98 (s, 3H). ^{1}H NMR (400 MHz, DMSO-d_6 (D_2O changed)) δ 7.79 (dd, J = 13.1, 8.5 Hz, 3H), 7.38 (t, J = 7.4 Hz, 1H), 7.28 (dd, J = 7.6, 4.7 Hz, 3H), 7.22 (d, J = 8.9 Hz, 1H), 7.14 (d, J = 8.3 Hz, 2H), 7.06 (s, 1H), 1.97 (s, 3H). FTIR (KBr pellets ν (cm^{-1})) 750, 814, 850, 1276, 1326, 1437, 1516, 1627, 3115, 3389.

N-[(2-Hydroxynaphthalene-1-yl)-(3-nitrophenyl)-methyl]-acetamide

^{1}H NMR (400 MHz, DMSO-d_6) δ 9.97 (s, 1H), 8.65 (d, J = 8.0 Hz, 1H), 8.06 (dt, J = 7.1, 2.2 Hz, 1H), 8.02 (s, 1H), 7.83 (t, J = 8.7 Hz, 3H), 7.61 – 7.53 (m, 3H), 7.42 (t, J = 7.8 Hz, 1H), 7.30 (t, J = 7.4 Hz, 1H), 7.24 (d, J = 8.8 Hz, 1H), 7.19 (d, J = 7.9 Hz, 1H), 2.03 (s, 3H). ^{1}H NMR (400 MHz, DMSO-d_6 (D_2O changed)) δ 8.04 (dt, J = 7.6, 2.1 Hz, 1H), 7.95 (d, J = 2.3 Hz, 1H), 7.90 – 7.78 (m, 3H), 7.61 – 7.52 (m, 2H), 7.42 (t, J = 7.8 Hz, 1H), 7.30 (t, J = 7.4 Hz, 1H), 7.22 (d, J = 8.9 Hz, 1H), 7.16 (s, 1H), 2.01 (s, 3H). FTIR (KBr pellets ν (cm^{-1})) 707, 808, 1206, 1436, 1347, 1520, 1644, 3206, 3372.

N-[(2-Hydroxynaphthalene-1-yl)-(4-methoxyphenyl)-methyl]-acetamide

^{1}H NMR (400 MHz, DMSO-d_6) δ 8.43 (d, J = 8.5 Hz, 1H), 7.84 (d, J = 7.6 Hz, 1H), 7.80 (d, J = 6.9 Hz, 1H), 7.76 (s, 1H), 7.36 (s, 1H), 7.25 (dd, J = 15.7, 8.2 Hz, 3H), 7.06 (t, J = 4.2 Hz, 3H), 6.82 – 6.80 (m, 2H), 3.69 (s, 3H), 1.96 (s, 3H). FTIR (KBr pellets ν (cm^{-1})) 750, 811, 822, 1117, 1250, 1438, 1516, 1626, 3056, 3394.

N-[(2-Hydroxynaphthalene-1-yl)-(2,4-di-chlorophenyl)-methyl]-acetamide

^{1}H NMR (400 MHz, DMSO-d_6) δ 8.63 (d, J = 7.9 Hz, 1H), 7.95 (d, J = 8.6 Hz, 1H), 7.80 (dd, J = 8.2, 1.4 Hz, 1H), 7.74 (d, J = 8.8 Hz, 1H), 7.59 (d, J = 8.5 Hz, 1H), 7.47 (d, J = 2.3 Hz, 1H), 7.46 – 7.40 (m, 2H), 7.28 (t, J = 7.5 Hz, 1H), 7.11 (d, J = 8.8 Hz, 1H), 6.99 (d, J = 7.7 Hz, 1H), 1.92 (s, 3H). FTIR (KBr pellets ν (cm^{-1})) 751, 813, 869, 1312, 1367, 1434, 1515, 1646, 3118, 3402.

N-[(2-Hydroxynaphthalene-1-yl)-(2-methoxyphenyl)-methyl]-acetamide

^{1}H NMR (400 MHz, DMSO-d_6) δ 9.5 (S,1H), 8.31 (d, J = 8.5 Hz, 1H), 8.16 (d, J = 8.7 Hz, 1H), 7.76 (dd, J = 8.1, 1.4 Hz, 1H), 7.68 (d, J = 8.8 Hz, 1H), 7.47 (d, J = 7.2 Hz, 1H), 7.41 (ddd, J = 8.5, 6.8, 1.4 Hz, 1H), 7.25 (dd, J = 7.9, 6.8 Hz, 1H), 7.18 (ddd, J = 8.2, 6.3, 4.8 Hz, 2H), 7.13 (d, J = 8.8 Hz, 1H), 6.91 – 6.85 (m, 2H), 3.58 (s, 3H), 1.89 (s, 3H). FTIR (KBr pellets ν (cm^{-1})) 753, 809, 850, 1263, 1327, 1443, 1513, 1624, 3067, 3429.

N-[(2-Hydroxynaphthalene-1-yl)-(3-nitrophenyl)-methyl]-chloroacetamide

^{1}H NMR (400 MHz, DMSO-d_6) δ 9.11 (d, J = 8.2 Hz, 1H), 8.11 – 8.04 (m, 2H), 7.94 (s, 1H), 7.89 – 7.82 (m, 2H), 7.60 (dt, J = 15.6, 7.8 Hz, 2H), 7.47 (t, J = 7.7 Hz, 1H), 7.32 (t, J = 7.5 Hz, 1H), 7.26 (d, J = 8.9 Hz, 1H), 7.17 (d, J = 7.7 Hz, 1H), 4.41 – 4.30 (m, 2H). ^{13}C NMR (101 MHz, DMSO-d_6) δ 166.72, 153.96, 148.26, 144.99, 133.28, 132.47, 130.64, 130.24, 129.25, 128.77, 127.56, 123.26, 122.78, 122.07, 120.88, 118.96, 117.39, 48.64, 43.18. FTIR (KBr pellets ν (cm^{-1})) 724, 779, 821, 1274, 1346, 1402, 1525, 1635, 3090, 3382.

N-[(2-Hydroxynaphthalene-1-yl)-(2-nitrophenyl)-methyl]-chloroacetamide

^{1}H NMR (400 MHz, DMSO-d_6) δ 8.99 (d, J = 8.3 Hz, 1H), 7.85 (s, 1H), 7.84 – 7.77 (m, 2H), 7.74 (dd, J = 8.5, 6.3 Hz, 2H), 7.68 (d, J = 4.4 Hz, 1H), 7.48 (ddd, J = 14.7, 9.4, 5.4 Hz, 3H), 7.29 (t, J = 7.4 Hz, 1H), 7.07 (d, J = 8.9 Hz, 1H), 4.28 (d, J = 12.9 Hz, 1H), 4.20 (d, J = 12.9 Hz, 1H). ^{13}C NMR (101 MHz, DMSO-d_6) δ 166.26, 154.37, 148.97, 136.42, 133.35, 132.55, 130.68, 129.22, 128.94, 128.47, 128.24, 127.23, 124.50, 123.03, 122.62, 118.90, 115.93, 46.38, 42.90. FTIR (KBr pellets ν (cm^{-1})) 732, 810, 852, 1277, 1353, 1401, 1526, 1640, 2123, 3381, 3500.

2.4 Characterization of the nanocatalyst

Crystalline structure of the prepared CNPO/CFO nanocatalyst was studied by X-ray diffraction (XRD) pattern using Philips X'pert Pro MPD, Cu Kα $\lambda = 1.54$ Å. Field emission scanning electron microscopy (FESEM) and energy dispersive X-ray (EDX) spectroscopy were employed to study the morphology and composition of the prepared nanocatalyst using TESCAN Mira 3. Fourier transform infrared (FTIR) spectroscopy was recorded to study the composition of the nanocatalyst and the functional groups of the amidoalkyl-2-naphthol derivatives. Also, the formation of metal phosphate structure was further investigated using Raman spectroscopy (Dilor LabRam-1B Raman spectrometer, excitation wavelength = 532 nm). Brunauer-Emmett-Teller (BET) analysis of the prepared catalysts was carried out at 77 K using BELsorp mini II, BEL, Japan. The vibrating sample magnetometer (VSM) analysis (VSM MDKB) was carried out to investigate the magnetic behavior of the synthesized CNPO/CFO nanocatalyst.

3. Results and discussion

3.1 Structure, morphology, and composition of the nanocatalyst

The XRD patterns for the prepared CNPO and CNPO/CFO are shown in Fig. 1. As can be seen in Fig. 1 (a), the diffraction peaks at 2θ = 29.2°, 30.3°, 35.7°, 38.9°, 41.9°, 43.7°, 48.6°, 52.6°, 53.9°, 54.7°, 58.1°, 59.6° and 63.9° correspond to the (012), (122), (220), (132), (131), (032), (133), (240), (033), (330), (400), (410) and (133) planes of monoclinic phase of CNPO (JCPDS file no. 048-0562). The organic compounds in the ginger extract such as the gingerol, which act as the stabilizing agent, restrict the particle growth process during the formation of the CNPO. As a consequence, the average crystallite size of particles is decreased by using the ginger extract. The Scherrer equation (Eq. 1) [38] was utilized to determine the average crystallite size for the prepared CNPO particles, as follows:

$$D = \frac{k\lambda}{\beta \cos\theta} \quad (1)$$

where D is the crystallite size, k is the shape factor (0.89), λ is the wavelength of the X-ray (Cu Kα = 1.54 Å), β is the width of the peak at half maximum (FWHM), and θ is the diffraction peak angle. As expected, the prepared CNPO in the presence of the ginger extract possesses a smaller crystallite size (35.7 nm) compared to those prepared in aqueous media (79.4 nm). Fig. 1 (b) exhibits the XRD patterns for the anchored CFO nanoparticles on the surface of CNPO particles. As seen from Fig. 1 (b), there are some diffraction peaks related to the CFO phase, JCPDS file no. 034-0425, (marked by ♣) along with assigned peaks for the CNPO phase (marked by ⊗).

Fig. 2 (a-d) shows the morphological properties of the prepared CNPO and CNPO/CFO samples. The FESEM image for the CNPO prepared by ginger, Fig. 2 (a), exhibits smaller and more uniform particles compared to those prepared in water media (Fig. 2 (b)). As clearly seen, the size distribution of particles is affected by the stabilizing nature of ginger extract. This result confirms the potential of organic compounds in ginger extract, such as gingerol, to stabilize the particles (scheme 2). In addition, Fig. 2 (c, d) represents the FESEM images for the anchored CFO on the surface of CNPO. Clearly, CFO nanoparticles are observed on the surface of CNPO.

EDX spectra for CNPO and CNPO/CFO are shown in Fig. S1 (a-b), which particularly disclose the components for the CNPO sample with relative amounts of Cu (22.45 wt%), Ni (18.23 wt%), P (21.91 wt%), and O (37.41 wt%). Also, the distribution of constituent elements of CNPO/CFO nanocatalyst was studied using elemental mapping EDX, shown in Fig. 3 (a-e).

The successful stabilization of the CNPO nanoparticles using the ginger extract was further confirmed by FT-IR analysis, as shown in Fig. 4 (a). The bands at 2952 and 1629 cm^{-1} are attributed to the C-H and C-O bonds [41], originating from the compounds in the ginger extract. The FT-IR spectrum for the calcined CNPO is shown in Fig. 4 (b). Obviously, there is a broad absorption peak at the range 3000 – 3400 cm^{-1}, which belongs to the stretching vibration of OH groups. The characteristic peaks assigned to the asymmetric and symmetric modes of PO_3 groups are centered at 1112 and 1010 cm^{-1}, respectively. Also, the intense absorption peaks at 764 and 661 cm^{-1} are attributed to the stretching vibration of P-O-P bridges [42]. The metal-oxide groups have an apparent absorption peak which is occurred at 470 cm^{-1} [42]. The phase structure of the prepared CNPO was further confirmed by Raman spectroscopy, as shown in Fig. 4 (b). The Raman spectra were recorded at room temperature in the wavenumber range of 300-1500 cm^{-1}. As can be seen from Fig. 4 (c), the strong Raman peak centered at 1056 cm^{-1} belongs to the symmetric stretching vibration of PO_3 groups, while the asymmetric stretching of PO_3 is observed at 1144 cm^{-1}.

The peak at 740 cm^{-1} is assigned to the symmetric vibration of P-O-P bridges, which is the characteristic Raman peak for the metal diphosphate compounds [43]. The asymmetric vibration mode of P-O-P is observed at 949 cm^{-1} [44]. In addition, all peaks below 600 cm^{-1} are related to the P-O-P deformation vibrations [45].

Due to the higher size uniformity of the catalyst prepared by ginger extract, more active sites would be available to catalyze the amidoalkyl-2-naphthol synthesis reaction. To confirm this result, the surface and pore size distribution of the catalyst were studied using the adsorption/desorption of nitrogen through BET analysis, as shown in figure 5. According to BET analysis results, the surface area for the catalyst prepared in the presence of ginger extract and aqueous media are 6.28 and 5.36 m^2/g, respectively. Also, insets to Fig. 5 show the pore size distribution, which reveals that the catalyst prepared using ginger extract has an average pore size of 19.49 nm, while the catalyst prepared in aqueous media possesses a mean pore size of 21.29 nm.

The room temperature M-H curve in Fig. 6 shows the magnetic behavior of the synthesized nanocatalyst with the saturation magnetization (Ms) of 40 emu/g. Also, the inset to Fig. 6 represents the coercivity (Hc) value of 50.34 Oe for the nanocatalyst, confirming the ferromagnetic properties of the CNPO/CFO nanocatalyst. The magnetic properties facilitate the effective separation of the nanocatalyst from the reaction media.

3.2 Optimization of the reaction conditions

In order to study the effect of particle size on the efficiency of the nanocatalyst, the synthesis reaction was individually tested using both the CNPO/CFO nanocatalyst prepared in the ginger extract and aqueous media. Under the same experimental conditions, the catalyst prepared using the ginger extract represents higher efficiency (97%) toward the synthesis of 1-amidoalkyl-2-naphthol. By comparison, the catalyst prepared in the aqueous media has the efficiency of about 88%. Hence, the optimization of temperature and time of reaction for the synthesis of 1-Amidoalkyl-2-naphthol derivatives was performed over the CNPO/CFO nanocatalyst prepared using the ginger extract. Table S1a-c provides the studied parameters to find optimal conditions giving rise to a higher yield for the synthesis of 1-amidoalkyl-2-napthol derivatives.

3.3 Synthesis of 1-amidoalkyl-2-naphthols using CNPO/CFO nanocatalyst

1-amidoalkyl-2-naphthols were synthesized using CNPO/CFO nanocatalyst through a three-component reaction involving 2-naphthol, amide, and aromatic aldehyde. Table 1 summarizes the obtaining data for the different synthesized 1-amidoalkyl-2-naphthol derivatives.

To calculate the turnover frequency (TOF) and turnover number (TON), the P-OH groups were considered as Brønsted acid active sites. Based on stoichiometric calculation, the molar amount of P-OH groups was found to be 2.026×10^{-4} mol. Accordingly, TON (Eq.2) and TOF (Eq.3) values were determined as follows:

$$\mathrm{TON} = \frac{\text{yield}}{2.026 \times 10^{-4}} \tag{2}$$

$$\mathrm{TOF} = \frac{\mathrm{TON}}{\text{reaction time (hour)}} \tag{3}$$

The synthesis of 1-amidoalkyl-2-naphthol derivatives was explored using various aldehydes bearing different functional groups. As summarized in Table 1, aldehydes containing electron-withdrawing groups afforded the corresponding products in higher yields and shorter reaction times compared to those bearing electron-donating groups.

This enhanced reactivity can be attributed to the electron-withdrawing substituents, which pull electron density away from the aromatic ring and the aldehyde group, thereby increasing the electrophilic character of the carbonyl carbon. Consequently, the aldehyde exhibits greater reactivity toward nucleophilic amines, leading to a more rapid imine formation step. Nevertheless, it is noteworthy that both electron-donating and electron-withdrawing groups are capable of promoting the reaction, although electron-withdrawing substituents consistently result in improved reaction efficiency and yield [46, 47].

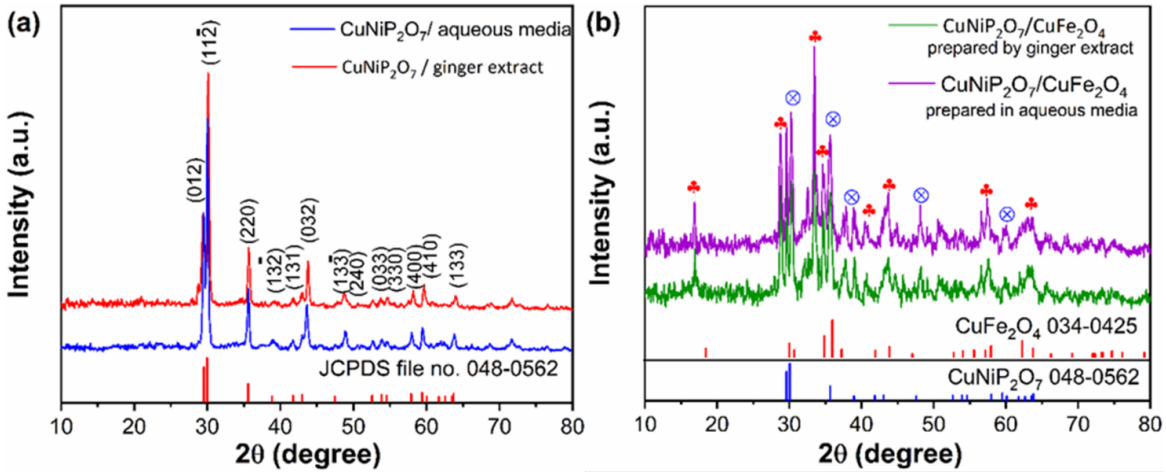

Figure 1. XRD patterns for the CNPO (a) and CNPO/CFO nanocatalyst (b).

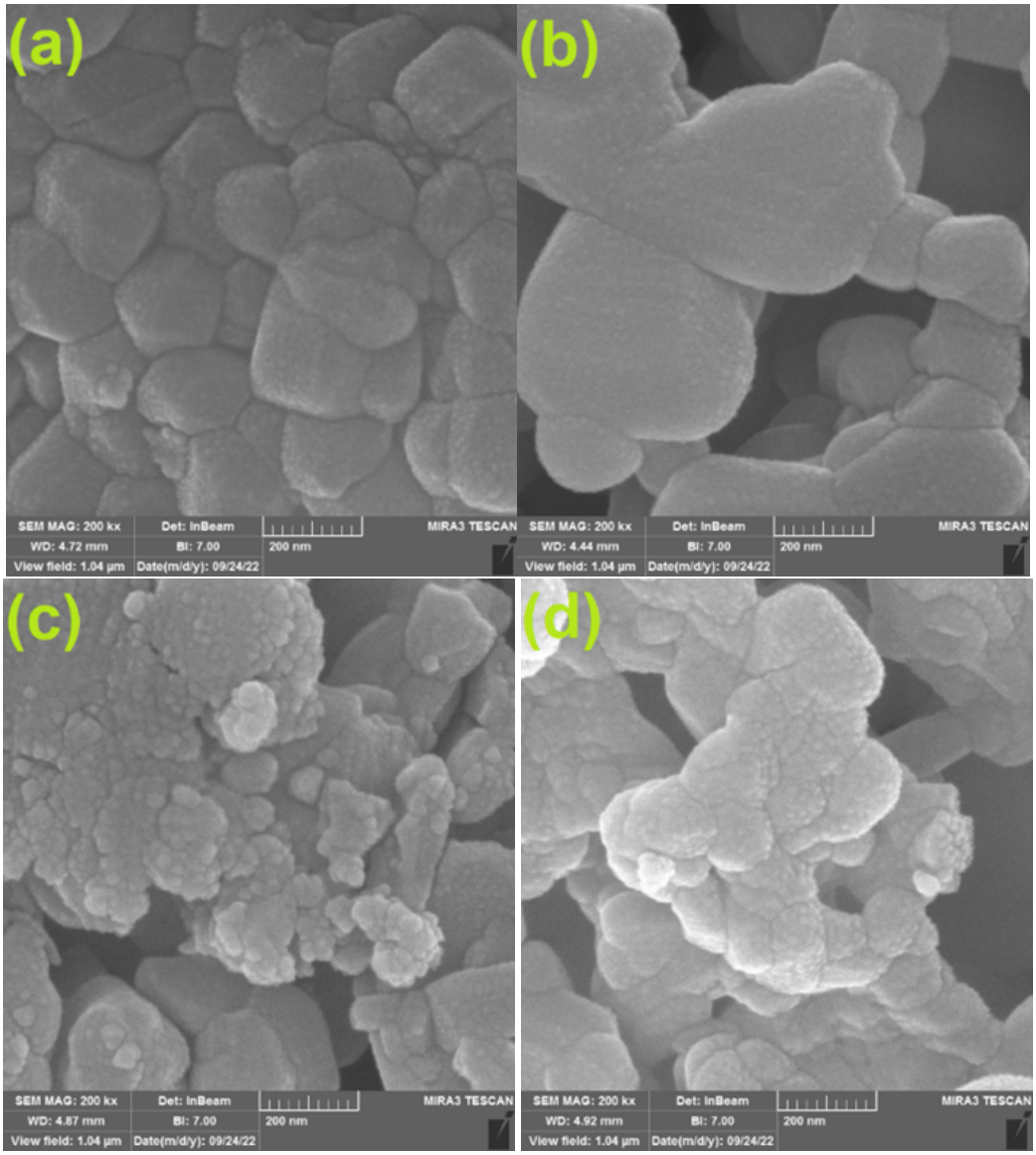

Figure 2. FESEM images for the CNPO: prepared in ginger extract (a) and aqueous media (b), and CNPO/CFO nanocatalyst: prepared in ginger extract (c) and aqueous media (d).

3.4 Proposed mechanism for catalytic synthesis of 1-Amidoalkyl-2-naphthol

The synthesis pathway of the 1-Amidoalkyl-2-naphthol over the prepared CNPO/CFO nanocatalyst is depicted in Fig. 7. The reaction is catalyzed via surface PO_4 groups serving as the Brønsted acid site. The existence of PO_4 groups on the surface of the prepared CNP particles was confirmed by FTIR analysis, shown in Fig. 4 (b). In the first step, the carbonyl group of aldehyde is activated by attaching to the Brønsted acid site, then the nucleophilic addition of β-naphthol is occurred by expelling H_2O. The formed intermediate is subsequently undergoes the Michael addition with the amide over the CNPO/CFO nanocatalyst to form the final product of 1-amidoalkyl-2-naphthol.

3.5 Reusability experiment

In order to study the reusability of the CNPO/CFO nanocatalyst (prepared using ginger extract) for the synthesis of 1-amidoalkyl-2-naphthol, the three-component reaction was conducted in 5 successive cycles. Each reaction cycle was carried out under the constant experimental conditions (T = 90 °C, amount of nanocatalyst = 0.04 g, and time = 10 min). After each reaction, the separated nanocatalyst was washed with methanol and deionized water four 4 times and then dried at 100 °C for 2 hours. The efficiency of the CNPO/CFO nanocatalyst was investigated by measuring the mass of the obtained solid product in each reaction cycle. Fig. 8 (a) is shown the results of the reusability experiment in 5 consecutive reaction cycles. As can be seen, the CNPO/CFO nanocatalyst discloses the excellent reusability even after 5 reaction cycles for synthesizing 1-amidoalkyl-2-naphthol. The loss of efficiency is negligible after 3 successive reactions (7%). However, a decline in the nanocatalyst efficiency in the five reaction cycles is about 13%. The reduction in the nanocatalyst efficiency is attributed to the detachment of CNPO from the CFO magnetic nanoparticles during the successive reactions. Figure 8 (b) shows the XRD patterns for the CNPO/CFO nanocatalyst before

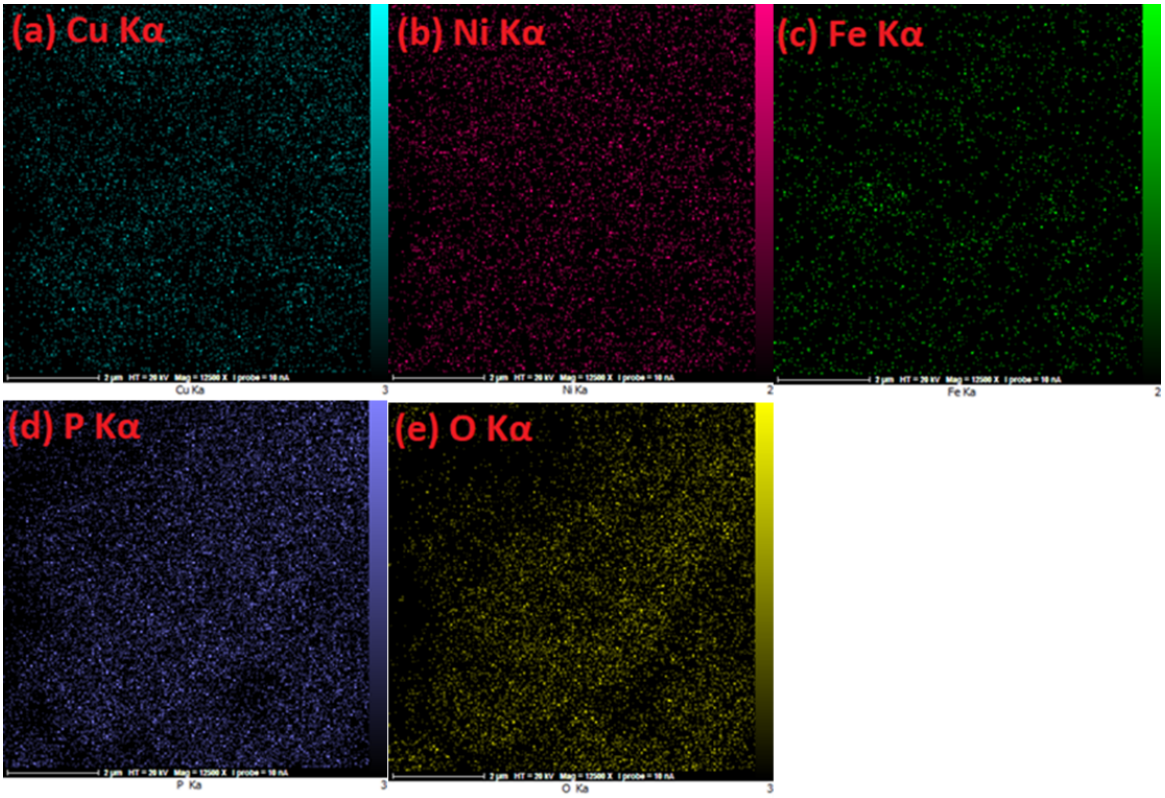

Figure 3. Element mapping Cu (a), Ni (b), Fe (c), P (d), O (e) for the prepared CNPO/CFO nanocatalyst.

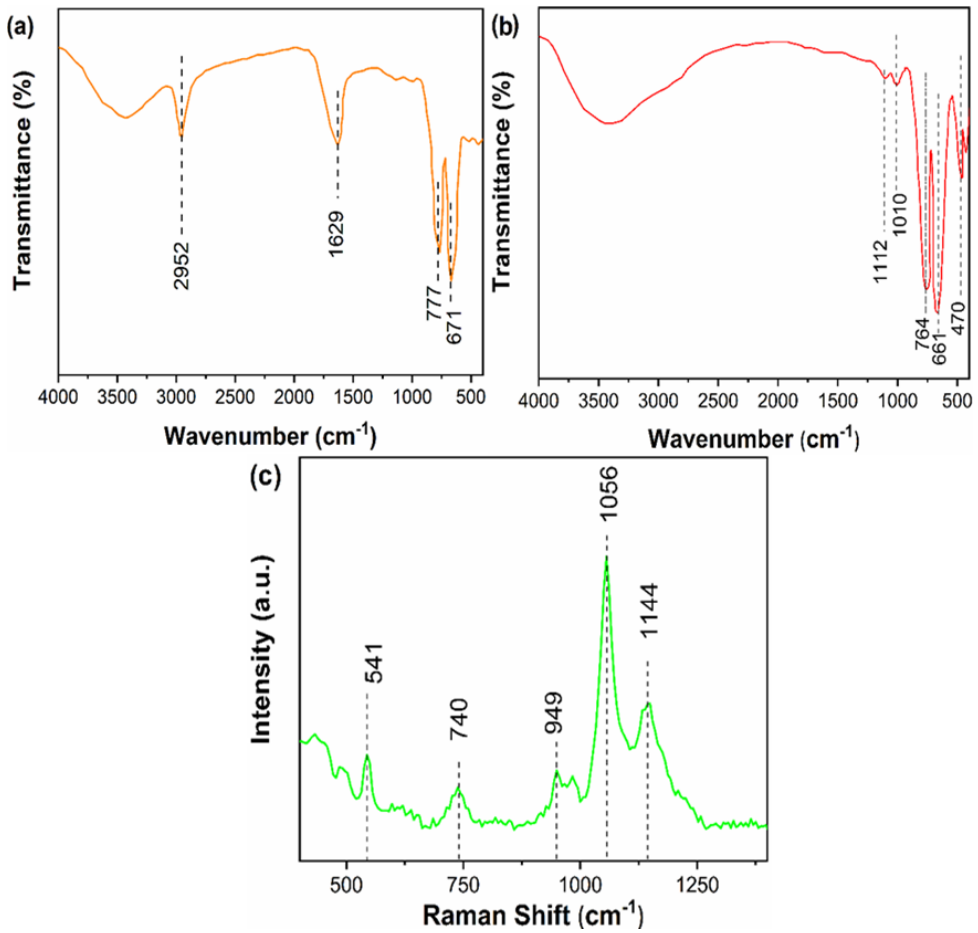

Figure 4. FT-IR spectra (a, b) and RAMAN (c) spectrum for the prepared CNPO.

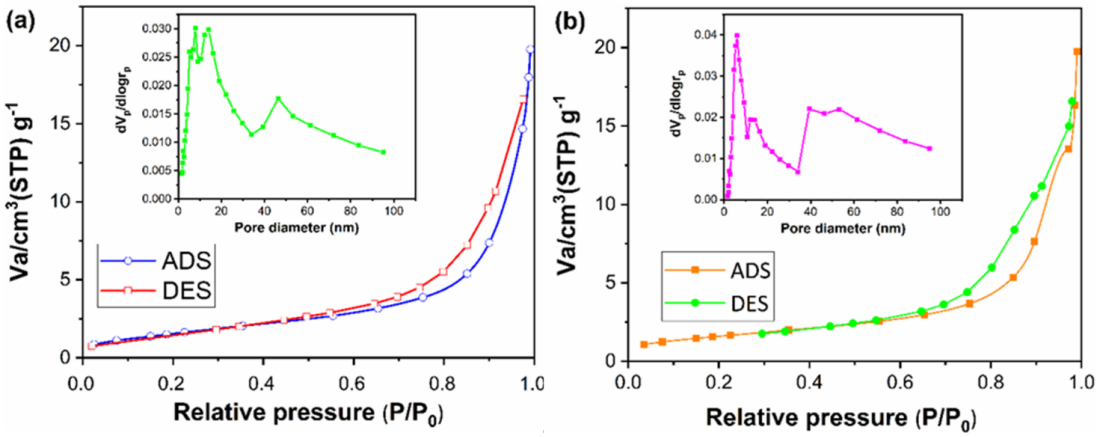

Figure 5. BET isotherm plots: and CNPO/CFO prepared using ginger extract (a) and aqueous media (b).

and after performing reusability experiments. As shown, the XRD patterns depict the decrease in the intensity of diffraction peaks, which correspond to the CNPO phase of the nanocatalyst, marked with ⊗.

The efficiency of the CNPO/CFO nanocatalyst for the synthesis of 1-amidoalkyl-2-naphthol was compared with that of catalysts reported in the previous literature. Table 2 is tabulated the experimental conditions for the synthesis of 1-amidoalkyl-2-naphthol using different catalysts.

3.6 Leaching test experiments

To validate the proceeding the synthesis reaction over the prepared heterogeneous nanocatalyst, the hot filtration test was conducted. For this purpose, 2 mmol of 2-naphthol, 1 mmol of benzamide, and 1 mmol of 3-ethoxy-4-hydroxybenzaldehyde (Entry 5, Table 1) were reacted in the presence of 0.04 g of CNPO/CFO nanocatalyst at a temperature of 90 °C. After 10 min, the catalyst was separated using a bar magnet, and the yield of the product was calculated to be 40%. Then, the reaction was continued in the absence of the catalyst for 15 min. The efficiency of the synthetic reaction was investigated once again, which showed no increase in the yield of the product. These results confirmed that the synthesis of the 1-amidoalkyl-2-naphthols is proceeded heterogeneously over the CNPO/CFO nanocatalyst.

4. Conclusion

In summary, we have prepared the CNPO as an efficient catalyst for promoting the synthesis of 1-amidoalkyl-2-naphthols. The simple and straight precipitation method was used to prepare CNPO. The ginger extract was used as a green stabilizing agent to control the size and uniformity of the CNPO particles. The surface of CNPO was also decorated with as-prepared CFO nanoparticles to form a magnetically separable nanocatalyst. 1-amidoalkyl-2-naphthol was synthesized via a three-component reaction over the CNPO/CFO nanocatalyst as the magnetically separable solid acid. The nanocatalyst reveals a great efficiency (97%) for the synthesis of 1-amidoalkyl-2-naphthol. The reusability experiment showed the excellent efficiency of the prepared nanocatalyst in 5 successive reactions.

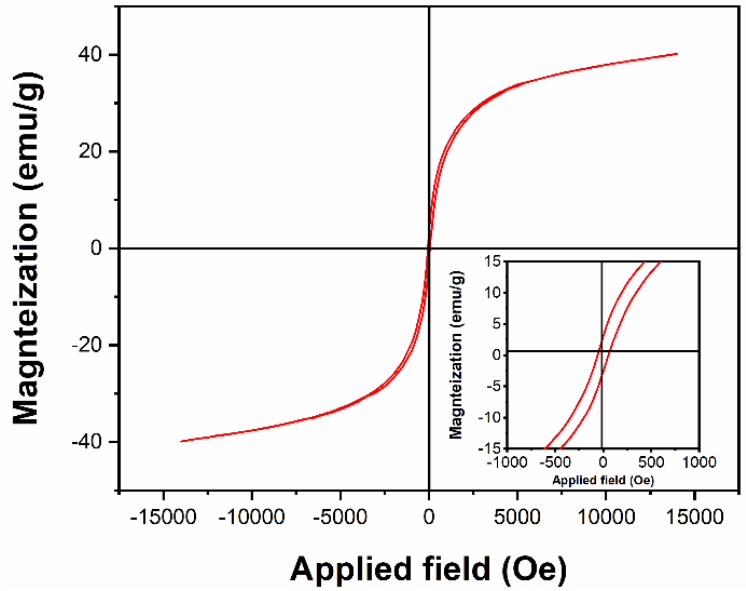

Figure 6. M-H curve for the synthesized CNPO/CFO nanocatalyst.

Table 1. Synthesis of different derivatives for 1-amidoalkyl-2-naphthol using CNPO/CFO nanocatalyst.

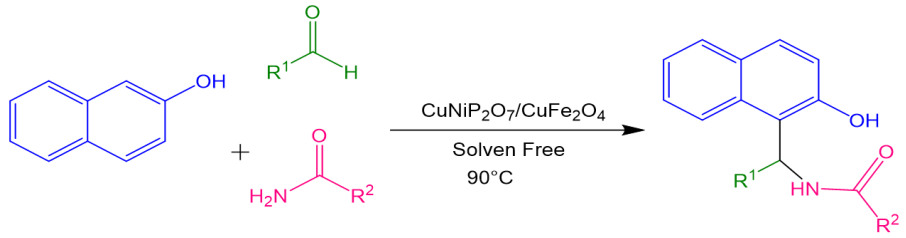

2 mmol of 2-naphthol, 1 mmol of aldehyde, 1 mmol of amide, Catalyst amount = 0.04 g, Solvent free condition.

Entry	Aldehyde	Amide	Product	Time (min)	Yield (%)	Melting point (°C)	TON ($\times 10^5$)	TOF ($\times 10^5$)	Ref.
1	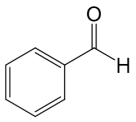	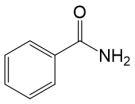	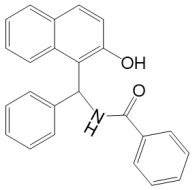	12	96	232-235	4.72	23.6	[34]
2	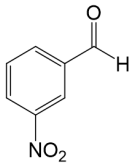	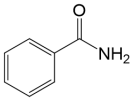	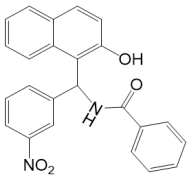	15	94	215-217	4.63	18.52	[35]
3	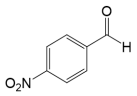	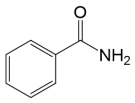	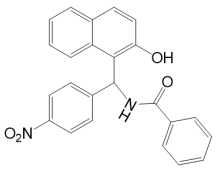	10	97	231-234	4.72	28.26	[34]
4	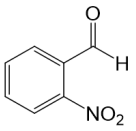	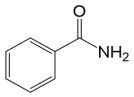	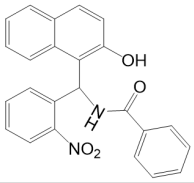	15	94	231-234	4.63	18.52	[35]
5	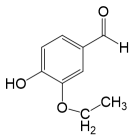	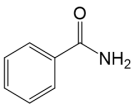	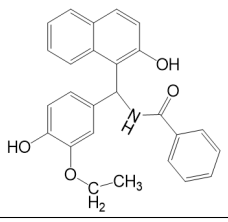	25	93	237-245	4.59	11.01	[36]
6	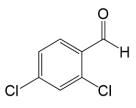	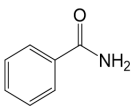	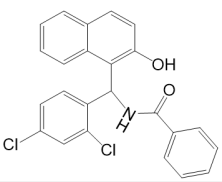	12	97	233-236	4.78	23.98	[35]
7	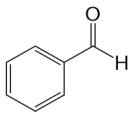	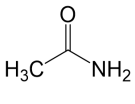	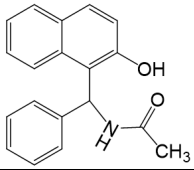	15	95	240-244	4.68	18.72	[37]

Continued of Table 1.

8	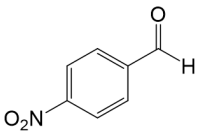	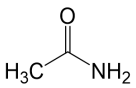	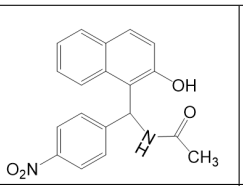	15	94	247-249	4.63	18.55	[35]
9	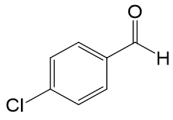	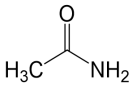	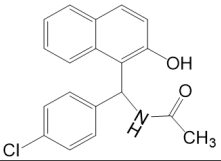	12	95	224-226	4.68	23.4	[37]
10	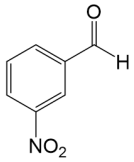	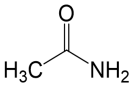	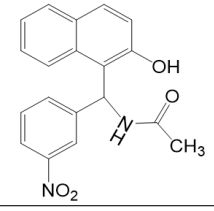	20	93	241-243	4.59	13.77	[37]
11	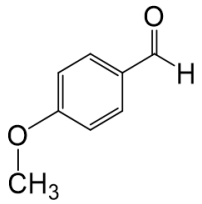	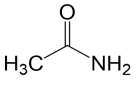	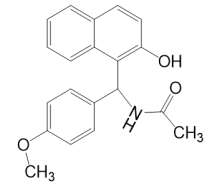	15	94	234-256	4.63	18.55	[35]
12	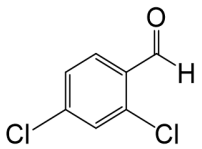	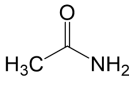	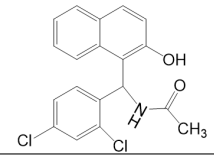	12	95	202-204	4.68	23.44	[39]
13	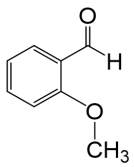	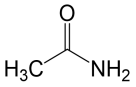	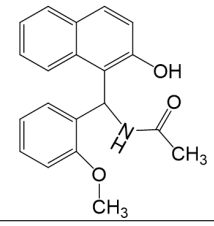	20	92	202-205	4.54	13.62	[37]
14	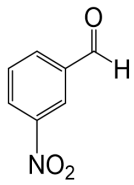	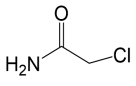	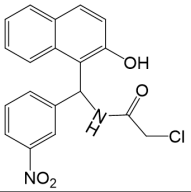	10	97	214-216	4.78	28.72	[40]
15	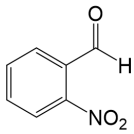	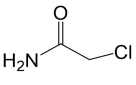	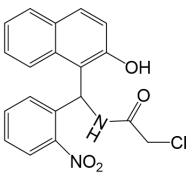	15	95	205-208	4.68	18.75	[40]

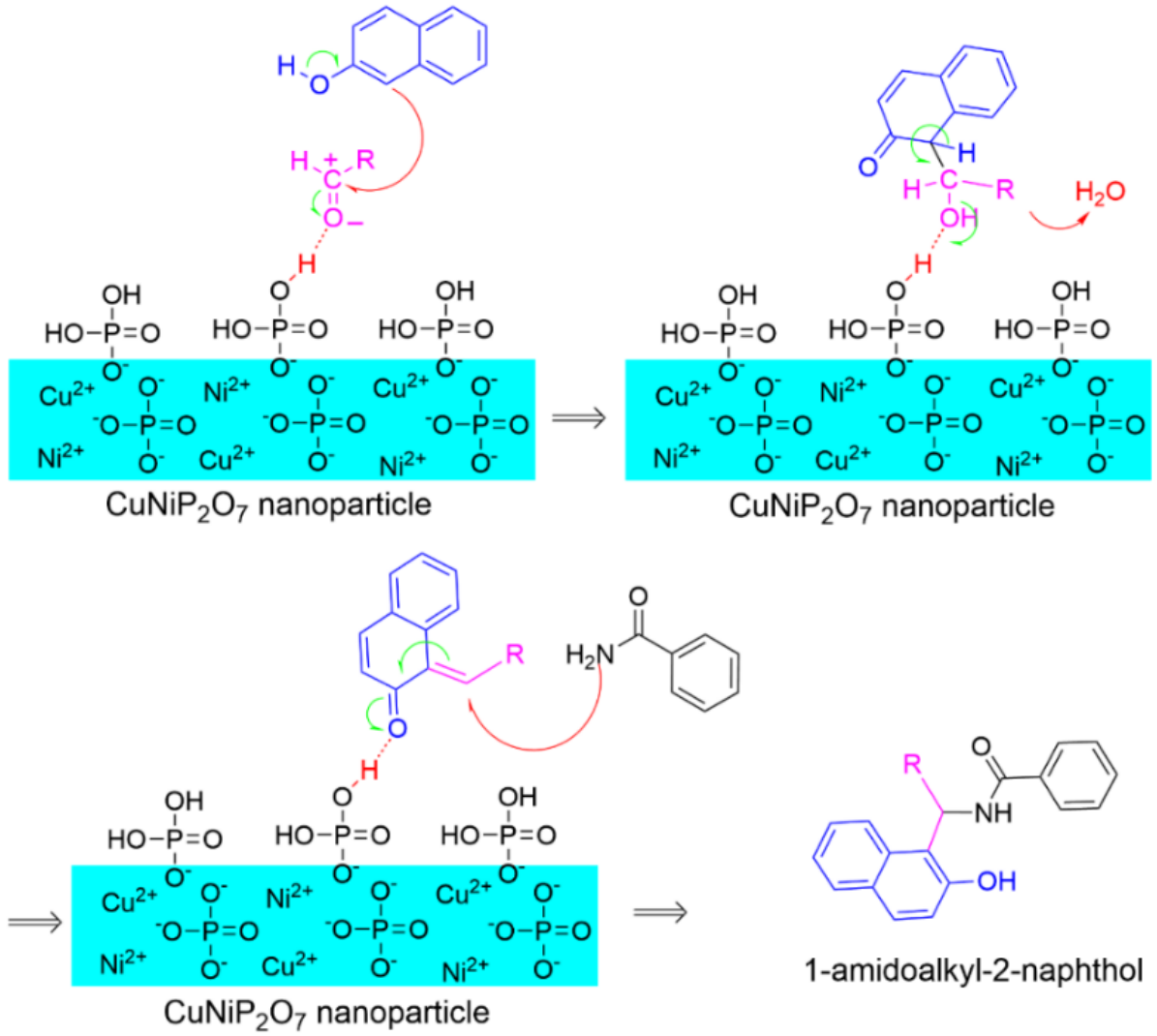

Figure 7. Proposed mechanism for synthesis of 1-amidoalkyl-2-naphthol over CNPO/CFO nanocatalyst.

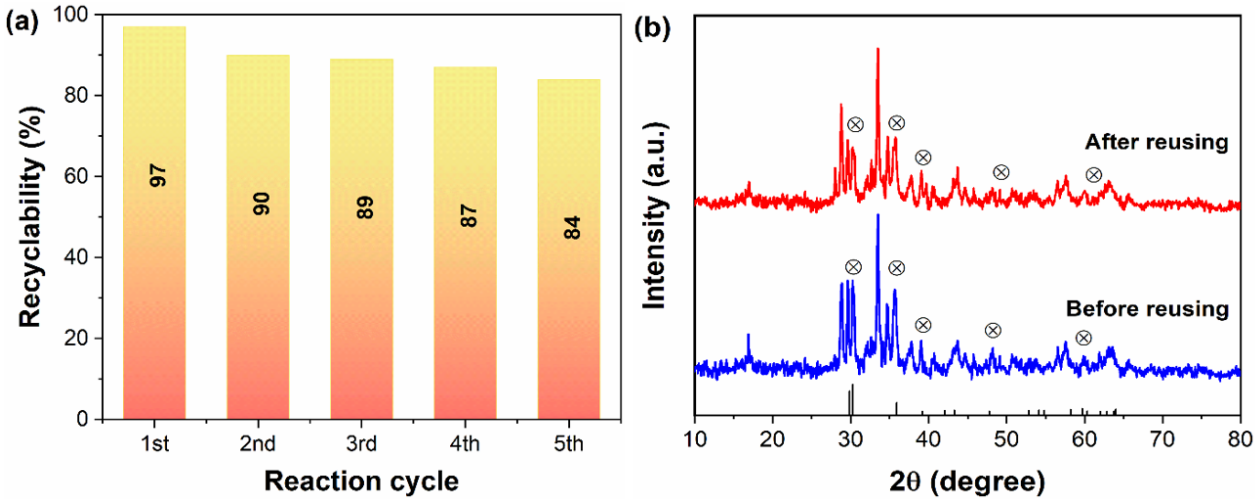

Figure 8. Recyclability experiments over CNPO/CFO nanocatalyst.

Table 2. Comparison of the catalytic efficiency of the CNPO/CFO with some reported catalysts for the synthesis of 1-amidoalkyl-2-naphtols in solvent-free conditions.

Catalyst	Catalyst amount	Time (min)	Temperature (°C)	Yield (%)	Ref.
CNPO/CFO	0.04 g	10	90	97	This work
Ag-TiO_2	2 mol%	30	110	92	[12]
Cu@Ag-CeO_2/Chitosan	0.01	15	100	98	[48]
CNT@Ni-bipy	0.01 g	8	100	95	[36]
Fe_3O_4@SiO_2@IL-PVP	0.02 g	15	80	95	[49]
B-cyclodextrin-butane sulfonic acid	1 mol%	6	100	90	[35]
$H_6P_2W_{18}O_{62}$/pyridine-Fe_3O_4	0.02 g	30	100	92	[50]
$K_5CoW_{12}O_{40}\cdot 3H_2O$	1 mol%	120	150	90	[51]
Polyphosphate ester	0.1 g	15	80	91	[52]
Note: bipy= bipyridine; IL-PVP= ionic liquid-polyvinylpyrrolidone.					

Acknowledgments
The authors would like to appreciate the financial support of this work by the University of Kashan, Iran.

Authors contributions
Authors have contributed equally in preparing and writing the manuscript.

Availability of data and materials
The data that support the findings of this study are available from the corresponding author, upon reasonable request.

Conflict of interests
The author declare that they have no known competing financial interests or personal relationships that could have appeared to influence the work reported in this paper.

References

[1] K. Boudebbous, H. Boulebd, C. Bensouici, D. Harakat, R. Boulcina, and A. Debache. *ChemistrySelect*, **5** (2020):5515–5520. DOI: https://doi.org/10.1002/slct.202000558.

[2] S. S. Dipake, S. P. Gadekar, P. B. Thombre, M. K. Lande, A. S. Rajbhoj, and S. T. Gaikwad. *Catal. Lett.*, **152** (2022):755–770. DOI: https://doi.org/10.1007/s10562-021-03684-8.

[3] H. Taghrir, M. Ghashang, and M. N. Biregan. *Chin. Chem. Lett.*, **27** (2016):119–126. DOI: https://doi.org/10.1016/j.cclet.2015.08.011.

[4] R. Tayebee, M. M. Amini, H. Rostamian, and A. Aliakbari. *Dalton Trans.*, **43** (2014):1550–1563, . DOI: https://doi.org/10.1039/C3DT51594J.

[5] G. Graziano, A. Stefanachi, M. Contino, R. Prieto-Díaz, A. Ligresti, P. Kumar, A. Scilimati, E. Sotelo, and F. Leonetti. *Int. J. Mol. Sci.*, **24** (2023):6581. DOI: https://doi.org/10.3390/ijms24076581.

[6] A. Dömling, W. Wang, and K. Wang. *Chem. Rev.*, **112** (2012):3083–3135. DOI: https://doi.org/10.1021/cr100233r.

[7] M. A. Bodaghifard and H. Allahbakhshi. *Colloid Nanosci. J.*, **2** (2024):238–253. DOI: https://doi.org/10.61186/CNJ.2.1.238.

[8] H. R. Shaterian, K. Azizi, and N. Fahimi. *Arab. J. Chem.*, **10** (2017): S42–S55, . DOI: https://doi.org/10.1016/j.arabjc.2012.07.006.

[9] H. R. Shaterian, H. Yarahmadi, and M. Ghashang. *Turk. J. Chem.*, **33** (2009):449–457, . DOI: https://doi.org/10.3906/kim-0812-67.

[10] M. A. Amrollahi, B. B. F. Mirjalili, and H. Emtiazi. *J. Chem. Sci.*, **125** (2013):561–566. DOI: https://doi.org/10.1007/s12039-013-0406-x.

[11] G. G. Patil, B. B. Muntode, N. K. Jadhav, V. A. Dhere, S. Khabnadideh, and R. R. Kale. *Curr. Organocatalysis*, **12** (2024). DOI: https://doi.org/10.2174/0122133372337451240923173335.

[12] S. Firozi, S. M. Vahdat, S. Khaksar, and M. Hatami. *Russ. J. Org. Chem.*, **60** (2024):131–137. DOI: https://doi.org/10.1134/S1070428024010172.

[13] J. Sang, P. Wei, T. Liu, H. Lv, X. Ni, D. Gao, J. Zhang, H. Li, Y. Zang, and F. Yang. *Angew. Chem.*, **134** (2022):e202114238. DOI: https://doi.org/10.1002/ange.202114238.

[14] A. Kumar and R. Srivastava. *ACS Sustain. Chem. Eng.*, **8** (2020): 9497–9506. DOI: https://doi.org/10.1021/acssuschemeng.0c02439.

[15] K. Nakajima, R. Noma, M. Kitano, and M. Hara. *J. Phys. Chem. C*, **117** (2013):16028–16033. DOI: https://doi.org/10.1021/jp404523r.

[16] L. Mitchell, P. Williamson, B. Ehrlichová, A. E. Anderson, V. R. Seymour, S. E. Ashbrook, N. Acerbi, L. M. Daniels, R. I. Walton, and M. L. Clarke. *Chem. Eur. J.*, **20** (2014):17185–17197. DOI: https://doi.org/10.1002/chem.201404377.

[17] D. Spielbauer, G. Mekhemer, T. Riemer, M. Zaki, and H. Knözinger. *J. Phys. Chem. B*, **101** (1997):4681–4688. DOI: https://doi.org/10.1021/jp963785x.

[18] R. Weingarten, Y. T. Kim, G. A. Tompsett, A. Fernández, K. S. Han, E. W. Hagaman, W. C. Conner Jr, J. A. Dumesic, and G. W. Huber. *J. Catal.*, **304** (2013):123–134, . DOI: https://doi.org/10.1016/j.jcat.2013.03.023.

[19] T. Rom, A. Agrawal, S. Sarkar, P. Mahata, A. Kumar, and A. K. Paul. *Inorg. Chem.*, **61** (2022):9580–9594. DOI: https://doi.org/10.1021/acs.inorgchem.2c00811.

[20] T. Zhou, Y. Du, D. Wang, S. Yin, W. Tu, Z. Chen, A. Borgna, and R. Xu. *ACS Catal.*, **7** (2017):6000–6007.
DOI: https://doi.org/10.1021/acscatal.7b00937.

[21] F. Li, L. J. France, Z. Cai, Y. Li, S. Liu, H. Lou, J. Long, and X. Li. *Appl. Catal. B: Environ.*, **214** (2017):67–77.
DOI: https://doi.org/10.1016/j.apcatb.2017.05.013.

[22] S. Wang, Z. Wang, and Z. Zha. *Dalton Trans.*, **43** (2009):9363–9373.
DOI: https://doi.org/10.1039/B913539A.

[23] Z. Guo, D. S. Theng, K. Y. Tang, L. Zhang, L. Huang, A. Borgna, and C. Wang. *Phys. Chem. Chem. Phys.*, **18** (2016):23746–23754.
DOI: https://doi.org/10.1039/C6CP04163A.

[24] R. Weingarten, Y. T. Kim, G. A. Tompsett, A. Fernández, K. S. Han, E. W. Hagaman, W. C. Conner, J. A. Dumesic, and G. W. Huber. *J. Catal.*, **304** (2013):123–134, .
DOI: https://doi.org/10.1016/j.jcat.2013.03.023.

[25] M. E. A. Drici, B. Amina, B. Redouane, B. Mohammed, B. Sumeya, and M. Debdab. *React. Kinet. Mech. Catal.*, **136** (2023):333–343.
DOI: https://doi.org/10.1007/s11144-023-02345-8.

[26] H. He, X. Shen, X. Ding, and J. C. Antilla. *Org. Lett.*, **25** (2023): 782–787.
DOI: https://doi.org/10.1021/acs.orglett.2c04277.

[27] H. Duan, D. Wang, and Y. Li. *Chem. Soc. Rev.*, **44** (2015):5778–5792.
DOI: https://doi.org/10.1039/C4CS00363B.

[28] S. Jadoun, R. Arif, N. K. Jangid, and R. K. Meena. *Environ. Chem. Lett.*, **19** (2021):355–375.
DOI: https://doi.org/10.1007/s10311-020-01074-x.

[29] P. Kurhade, S. Kodape, and R. Choudhury. *Chem. Pap.*, **75** (2021): 5187–5222.
DOI: https://doi.org/10.1007/s11696-021-01693-w.

[30] R. B. Semwal, D. K. Semwal, S. Combrinck, and A. M. Viljoen. *Phytochem.*, **117** (2015):554–568.
DOI: https://doi.org/10.1016/j.phytochem.2015.07.012.

[31] A. A. El-Refai, G. A. Ghoniem, A. Y. El-Khateeb, and M. M. Hassaan. *J. Nanostructure Chem.*, **8** (2018):71–81.
DOI: https://doi.org/10.1007/s40097-018-0255-8.

[32] M. Yadi, M. Azizi, H. Dianat-Moghadam, A. Akbarzadeh, M. Abyadeh, and M. Milani. *Bioprocess Biosyst. Eng.*, **45** (2022): 1905–1917.
DOI: https://doi.org/10.1007/s00449-022-02780-2.

[33] M. Chaani and J. Saffari. *J. Nanostruct.*, **6** (2016):172–178.
DOI: https://doi.org/10.7508/jns.2016.02.010.

[34] M. M. Khodaei, A. R. Khosropour, and H. Moghanian. *Synlett*, **6** (2006):916–920.
DOI: https://doi.org/10.1055/s-2006-939034.

[35] K. Gong, H. Wang, X. Ren, Y. Wang, and J. Chen. *Green Chem.*, **17** (2015):3141–3147.
DOI: https://doi.org/10.1039/C5GC00384A.

[36] J. Rakhtshah, H. Ghaderi, F. Yaghoobi, S. Baghery, and B. Shaabani. *Mater. Chem. Phys.*, **239** (2020):121985.
DOI: https://doi.org/10.1016/j.matchemphys.2019.121985.

[37] H. R. Shaterian and H. Yarahmadi. *Tetrahedron Lett.*, **49** (2008): 1297–1300.
DOI: https://doi.org/10.1016/j.tetlet.2007.12.093.

[38] C. F. Holder and R. E. Schaak. *ACS Nano*, **13** (2019):7359–7365.
DOI: https://doi.org/10.1021/acsnano.9b05157.

[39] S. Kantevari, S. V. Vuppalapati, and L. Nagarapu. *Catal. commun.*, **8** (2007):1857–1862.
DOI: https://doi.org/10.1016/j.catcom.2007.02.022.

[40] H. A. Soliman, A. Y. Mubarak, A. El-Mekabaty, H. M. Awad, and S. S. Elmorsy. *Monatsh. Chem.*, **147** (2016):809–816.
DOI: https://doi.org/10.1007/s00706-015-1536-2.

[41] A. S. Beheshtian, M. H. Givianrad, H.-A. Rafiee-Pour, and P. A. Azar. *Opt. Quantum Electron.*, **55** (2023):463.
DOI: https://doi.org/10.1007/s11082-023-04729-5.

[42] M. Moutataouia, F. El bachraoui, Y. Tamraoui, M. Lamire, S. Krimi, and B. Manoun. *J. Mol. Struct.*, **1223** (2021):128983.
DOI: https://doi.org/10.1016/j.molstruc.2020.128983.

[43] R. L. Frost. *Spectrochim. Acta A*, **60** (2004):1439–1445.
DOI: https://doi.org/10.1016/j.saa.2003.08.009.

[44] Y. Yang, P. Gong, S. Luo, Q. Huang, and Z. Lin. *J. Alloys Compd.*, **744** (2018):370–374.
DOI: https://doi.org/10.1016/j.jallcom.2018.02.113.

[45] Y. Inomata, T. Inomata, and T. Moriwaki. *Spectrochim. Acta A*, **36** (1980):839–842.
DOI: https://doi.org/10.1016/0584-8539(80)80083-3.

[46] Z. Karimi-Jaberi, M. Jokar, and S. Z. Abbasi. *J. Chem.*, **2013** (2013): 341649.
DOI: https://doi.org/10.1155/2013/341649.

[47] H. Petkov and S. P. Simeonov. *Appl. Sci.*, **13** (2023):6616.
DOI: https://doi.org/10.3390/app13116616.

[48] A. Mahajan, A. Mahajan, A. Kuznetsov, and M. Gupta. *ACS Sustain. Chem. Eng.*, **12** (2024):3419–3438.
DOI: https://doi.org/10.1021/acssuschemeng.3c05011.

[49] S. Vaysipour, M. Nasr-Esfahani, and Z. Rafiee. *Appl. Organomet. Chem.*, **33** (2019):e5090.
DOI: https://doi.org/10.1002/aoc.5090.

[50] R. Tayebee, M. M. Amini, H. Rostamian, and A. Aliakbari. *Dalton Trans.*, **43** (2014):1550–1563, .
DOI: https://doi.org/10.1039/C3DT51594J.

[51] L. Nagarapu, M. Baseeruddin, S. Apuri, and S. Kantevari. *Catal. Commun.*, **8** (2007):1729–1734.
DOI: https://doi.org/10.1016/j.catcom.2007.02.008.

[52] H. Moghanian and S. Ebrahimi. *J. Saudi Chem. Soc.*, **18** (2014): 165–168.
DOI: https://doi.org/10.1016/j.jscs.2011.06.017.